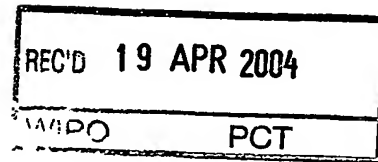


PCT/NZ2004/000060



CERTIFICATE

This certificate is issued in support of an application for Patent registration in a country outside New Zealand pursuant to the Patents Act 1953 and the Regulations thereunder.

I hereby certify that annexed is a true copy of the Provisional Specification as filed on 25 March 2003 with an application for Letters Patent number 524929 made by INDUSTRIAL RESEARCH LIMITED.

Dated 31 March 2004.

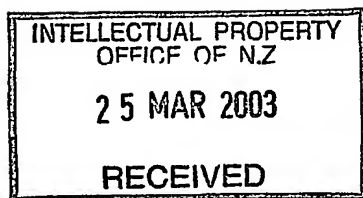
PRIORITY DOCUMENT
SUBMITTED OR TRANSMITTED IN
COMPLIANCE WITH
RULE 17.1(a) OR (b)

A handwritten signature in cursive script that reads "Neville Harris".

Neville Harris
Commissioner of Patents, Trade Marks and Designs



524929



NEW ZEALAND PATENTS ACT 1953

PROVISIONAL SPECIFICATION

NARROWBAND INTERFERENCE SUPPRESSION FOR PILOT SYMBOL ASSISTED OFDM SYSTEMS

We, INDUSTRIAL RESEARCH LIMITED, a New Zealand company, of Brooke House, 24 Balfour Road, Parnell, Auckland, New Zealand, do hereby declare this invention to be described in the following statement:

FIELD OF INVENTION

The invention relates to receivers for wireless communication and in particular to adaptive cancellation of narrowband interference in pilot symbol assisted OFDM receivers.

BACKGROUND

Orthogonal frequency division multiplexing (OFDM) has become the physical layer of choice for many wireless communications systems. Current wireless local area network (WLAN) and wireless metropolitan area network (WMAN) standards employ pilot symbols to aid detection and synchronization in the OFDM receiver. OFDM previously has been reported to be particularly sensitive to errors due to imperfect synchronization.

Pilot symbol assisted detection synchronization for OFDM relies on repeated pseudo-random binary sequences (PRBSs) being embedded in the pilot symbols, which are designed to have near-optimal unity peak to average power ratios (PAPRs) in both the time and frequency domain. Common approaches to pilot symbol assisted detection (and time offset estimation) are based on the correlation properties of the repeated PRBS in the pilot symbol. Similarly, the common approach to pilot symbol assisted synchronization (carrier frequency offset estimation) is based on exploiting the property that any frequency shift is common to the repeated PRBSs.

The susceptibility of pilot symbol assisted receivers to narrowband interference, with particular regard to OFDM systems is of particular importance as both WLAN and WMAN systems currently operate in unlicensed spectrum and therefore must co-exist with other unlicensed systems including cordless telephones, garage door openers, baby monitors and microwave ovens. Further, radio non-idealities such as transmitter carrier feedthrough (also known as carrier leakage) also introduce narrowband interference in the form of single-tone carrier residues. Previous work has proposed interference suppression using pre-coding. As well as this post-detection receiver techniques involving equalizers to improve bit error rate performance have been proposed.

A common model for a received, baseband (low pass equivalent) OFDM symbol, sampled with period T , is

$$r_n = as(nT - \tau_s) e^{-j[2\pi\nu(nT - \tau_s) + \theta]} + \eta(nT), \quad (1)$$

where a is the flat fading channel amplitude, $s(t)$ is the transmitted signal, n is the sample index, τ_s , ν and θ are the time-, frequency- and phase-offsets between transmitter and receiver introduced by a combination of system non-idealities and channel distortions, and η is complex additive white Gaussian noise (AWGN) having variance σ_w^2 . This model requires a number of assumptions including that the multipath channel is frequency non-selective (flat) and that the multipath channel is non time-varying (static). As the focus is on pilot symbol detection and frequency offset estimation, which are insensitive to sub-sample timing, the simplification $\tau_s=0$ is made here without loss of generality.

Consideration of narrowband interference using this model produces

$$r_n = as(nT) e^{-j[2\pi\nu nT + \theta]} + be^{-j[2\pi\xi nT + \phi]} + \eta(nT), \quad (2)$$

where b , ξ and ϕ are, respectively, the amplitude, frequency and phase of the *demodulated* narrowband interferer. Carrier feedthrough in the transmitter produces an in-band interferer at a frequency equal to the frequency difference between transmitter and receiver local oscillators which, depending on the amount of Doppler shift, will be equal or close to the signal frequency offset ν . Typically, the maximum carrier frequency offset is much less than the OFDM sub-carrier spacing and the pilot symbol is designed specifically to be able to resolve this frequency without ambiguity. Any DC offset will occur at $\xi=0$ and interference from other users of license-free spectrum may occur either singly (e.g. garage door openers, baby monitors, microwave ovens) or in pairs (e.g. cordless telephones) at any in-band frequency.

Pilot symbols for OFDM WLAN and WMAN standards comprise at least two repeated PRBSs, where each PRBS is of length L samples. While different receiver techniques are required for pilot symbol assisted detection and synchronization, depending on the number of PRBSs (including combinations of short and long PRBSs), all algorithms are based on the correlation properties between the repeated sequences.

The l th output sample of an L -length sliding window integrate-and-dump cross-correlator is

$$P_l = \mathbf{r}_l^H \mathbf{r}_{l+L}, \quad (3)$$

where $\mathbf{r} \triangleq [r_l, r_{l+1}, \dots, r_{l+L-1}]^T$ and $[\cdot]^H$ denotes Hermitian transpose. For a packet consisting of a pilot symbol preceded ($l < 0$) and followed ($l > 2L-1$) by noise only, analyses of P_l in an interference-free environment show that $|P_l|$ rises steeply to a peak (at $l=0$) before falling steeply to the noise-only level. Further, normalising $|P_l|$ produces the non-central correlation coefficient

$$|\rho_l| \triangleq \frac{|P_l|}{\sqrt{R_l R_{l+L}}} \quad (4)$$

where

$$R_l \triangleq \mathbf{r}_l^H \mathbf{r}_l \quad (5)$$

and the range of $|\rho_l|$ is constrained to $[0 \ 1]$. The receiver will declare a pilot symbol detection at the point where some threshold of correlation, T_C , is exceeded, that is when

$$|\rho_l| > T_C. \quad (6)$$

Detection becomes more complicated where pilot symbols comprise more than two PRBSs, include a cyclic prefix (guard interval) and apply matched filter techniques to increase timing resolution and minimise false detection probability. However, the comparison specified by equation (6) is fundamental in every case.

In an environment with a narrowband interferer substitution of equation (2) into equation (3) yields

$$\begin{aligned} P_l = & La^2 S^2 e^{-j2\pi\nu LT} + Lb^2 e^{-j2\pi\xi LT} \\ & + LaSb \left[e^{-j2\pi\nu LT} \Xi_l(\nu - \xi) + e^{-j2\pi\xi LT} \Xi_l^*(\nu - \xi) \right] \\ & + \boldsymbol{\eta}_l^H (a\mathbf{s}_{l+L} + b\xi_{l+L}) + (a\mathbf{s}_l^H + b\xi_l^H) \boldsymbol{\eta}_{l+L} + \boldsymbol{\eta}_l^H \boldsymbol{\eta}_{l+L}, \end{aligned} \quad (7)$$

where $\Xi_l(x) \triangleq e^{-j[2\pi xT + \theta - \phi]} \Phi(x)$ for $\Phi(x) \triangleq \frac{1}{SL} \sum_{m=0}^{L-1} s_{l+m} e^{-j2\pi x m T}$,

$$\mathbf{s}_l \triangleq e^{-j[2\pi\nu T + \theta]} [s_l, s_{l+1} e^{-j2\pi\nu T}, \dots, s_{l+L-1} e^{-j2\pi\nu(L-1)T}]^T,$$

$$\xi_l \triangleq e^{-j[2\pi\xi T + \phi]} [1, e^{-j2\pi\xi T}, \dots, e^{-j2\pi\xi(L-1)T}]^T \text{ and } S \text{ is the mean magnitude of the PRBS.}$$

Similarly, insertion of equation (2) into equation (5) yields

$$\begin{aligned}
R_I &= La^2S^2 + Lb^2 \\
&+ LaSb \left[\Xi_I (\nu - \xi) + \Xi_I^* (\nu - \xi) \right] \\
&+ \boldsymbol{\eta}_I^H (a\mathbf{s}_I + b\boldsymbol{\xi}_I) + (a\mathbf{s}_I^H + b\boldsymbol{\xi}_I^H) \boldsymbol{\eta}_I + \boldsymbol{\eta}_I^H \boldsymbol{\eta}_I.
\end{aligned} \tag{8}$$

In the absence of signal, that is, in a narrowband interferer plus noise only environment, the probability of false pilot symbol detection may be evaluated as follows. Simplification of equation (7) and equation (8) leads to the approximations

$$P_I \approx \underbrace{Lb^2 e^{-J2\pi\xi LT}}_{\text{interference term}} + \underbrace{\sqrt{L(b^2 + \sigma_w^2)} \eta_I}_{\text{composite noise term}}, \tag{9}$$

and

$$R_I \approx \underbrace{L(b^2 + 2\sigma_w^2)}_{\text{interference term}} + \underbrace{2\sqrt{L(b^2 + \sigma_w^2)} \text{Re}\{\eta_I\}}_{\text{composite noise term}}, \tag{10}$$

respectively, where η_I is a zero mean complex Gaussian random variable with variance σ_w^2 . Details of the approximations may be inferred by reference to A.J. Coulson, "Maximum Likelihood Synchronization for OFDM Using a Pilot Symbol: Algorithms", IEEE J. Selected Areas in Communications, vol. 19, no.12, pp 2486 – 2494, December 2001.

Evaluation of the false detection probability $p(|\rho_I| > T_c) \equiv p(|P_I|^2 - T_c^2 R_I^2 > 0)$ in a narrowband interference-only environment may be found by comparison with expressions found in A.J. Coulson, "Maximum Likelihood Synchronization for OFDM Using a Pilot Symbol: Analysis", IEEE J. Selected Areas in Communications, vol. 19, no.12, pp 2495 – 2503, December 2001. It is sufficient for the purposes here to examine

$$\begin{aligned}
\langle |\rho_I| \rangle &= \frac{\langle |P_I| \rangle}{\langle \sqrt{R_I R_{I+L}} \rangle} \\
&= \sqrt{\frac{\Gamma^2 + 1/L(2\Gamma + 1)}{(\Gamma + 1)^2 + 1/L(2\Gamma + 1)}} \approx \frac{\Gamma}{\Gamma + 1},
\end{aligned} \tag{11}$$

where $\langle \cdot \rangle$ denotes the expected value, $\Gamma \doteq b^2 / 2\sigma_w^2$ is the interference to noise ratio, and noting that equation (11) is independent of the output of the cross-correlator l since both the magnitude of the narrowband interferer and the statistics of AWGN (additive white Gaussian noise) are time-invariant. The approximation is accurate for large values of L and for $\Gamma \neq 0$.

From equation (11) it is clear that the non-central correlation coefficient $|\rho_l|$ will approach any practical value of T_C , even at modest levels of interference. For example, the commonly-used value of $T_C^2=0.8$ will be exceeded, on average, by a narrowband interferer only 9dB above the receiver noise floor. This means that a narrowband interferer will "swamp" a correlation-based detector based on equation (6), making it difficult to distinguish between the interference-only signal and an incoming pilot symbol, even though the pilot symbol may be tens of decibels greater in power than the interferer. More robust detection techniques, for example using a two-stage process employing a matched filter also will fail as a reasonably accurate forward estimate of frequency offset is required to produce the matched filter.

Frequency offset estimation is based on evaluating $\arg(P_l)$. Frequency offset estimation in the presence of narrowband interference but absence of signal will produce only an estimate of the carrier frequency of the interferer, which will be aliased if the carrier frequency is greater than the pilot symbol PRBS period inverse. In the presence of both signal and interference, the frequency offset estimate has an expected value of

$$\begin{aligned} \langle \hat{\nu} \rangle &\doteq \frac{1}{2\pi LT} \langle \arg(P_0) \rangle \\ &= \frac{1}{2\pi LT} \left\langle \arg \left(La^2 S^2 e^{-j2\pi \nu LT} + Lb^2 e^{-j2\pi \xi LT} + LaSb \left[e^{-j2\pi \nu LT} \Xi_l(\nu - \xi) + e^{-j2\pi \xi LT} \Xi_l^*(\nu - \xi) \right] \right) \right\rangle_{l=0} \end{aligned} \quad (12)$$

After some manipulations, the frequency offset estimation bias can be shown to have an expected value of

$$\begin{aligned}\phi_{bias} &\doteq \langle \hat{\nu} \rangle - \nu \\ &= \frac{1}{2\pi LT} a \tan \left(\frac{\sin[2\pi(\nu - \xi)LT] + 2\iota XY \sin[\pi(\nu - \xi)LT]}{\iota^2 + \cos[2\pi(\nu - \xi)LT] + 2\iota XY \cos[\pi(\nu - \xi)LT]} \right)\end{aligned}\quad (13)$$

where $\iota \doteq aS/b$ is the signal-to-interferer ratio, $X \doteq |\Phi(\nu - \xi)|$, $\chi \doteq \arg(\Phi(\nu - \xi))$ and $Y \doteq \cos[\theta - \phi + \chi + \pi(\nu - \xi)LT]$.

Clearly, the value of this bias significantly depends on the difference between the pilot symbol frequency offset and the interferer carrier frequency ($\nu - \xi$), the signal-to-interferer ratio, ι , and the properties of the PRBS, manifested through $\Phi(\nu - \xi)$. Of primary importance is that the bias depends on the *difference* $\nu - \xi$, rather than the frequency offset, ν , itself. Thus, for an interferer having a large carrier frequency ξ , the estimation bias ϕ_{bias} can significantly exceed ν itself even for a large signal-to-interference ratio, as illustrated in Figure 1.

An alternative "detection metric" to that of equation (4) has been proposed. This is the central correlation coefficient

$$|\rho_l'| \doteq \frac{|P_l'|}{\sqrt{R_l' R_{l+L}'}} \quad (14)$$

where

$$\begin{aligned}P_l' &\doteq (\mathbf{r}_l^H - \bar{\mathbf{r}}_l^*)(\mathbf{r}_{l+L} - \bar{\mathbf{r}}_{l+L}) \\ &= \mathbf{r}_l^H \mathbf{r}_{l+L} - L \bar{\mathbf{r}}_l^* \bar{\mathbf{r}}_{l+L}\end{aligned}\quad (15)$$

for $\bar{\mathbf{r}}_l \doteq \frac{1}{L} \sum_{m=0}^{L-1} \mathbf{r}_{l+m}$ and

$$R_l' \doteq \mathbf{r}_l^H \mathbf{r}_l - L \bar{\mathbf{r}}_l^* \bar{\mathbf{r}}_l \quad (16)$$

noting that, in contrast with normal practice, $'$ is used here to denote central moments and central random variables to maintain consistency with previously used notation. Intuitively, it is expected that the central correlation "detection metric" of equation (14) is more robust than the traditional non-central correlation coefficient of equation (4) in the presence of a near DC narrowband interferer.

In a narrowband interference-only environment, by inserting equations (7) and (8) into equations (15) and (16), and then into equation (14), the expected value of $|\rho'_l|$ can be shown to be

$$\begin{aligned} \langle |\rho'_l| \rangle &= \frac{\langle |P'_l| \rangle}{\langle \sqrt{R'_l R'_{l+L}} \rangle} \\ &= \sqrt{\frac{\tilde{\Gamma}^2 + 1/L(2\tilde{\Gamma} + 1)}{(\tilde{\Gamma} + 1)^2 + 1/L(2\tilde{\Gamma} + 1)}} \approx \frac{\tilde{\Gamma}}{\tilde{\Gamma} + 1}, \end{aligned} \quad (17)$$

where $\tilde{\Gamma} \triangleq (1 - |\Psi(\xi)|^2) b^2 / 2\sigma_w^2$ is the modified interference to noise ratio for $\Psi(\xi) \triangleq e^{j\pi\xi(L-1)T} \frac{\sin \pi\xi LT}{L \sin \pi\xi T}$, and the approximation is accurate for large values of L and for $\tilde{\Gamma} \neq 0$. Note that, as with $\langle |\rho_l| \rangle$, $\langle |\rho'_l| \rangle$ is independent of l in the absence of a signal.

The mean improvement in interference rejection gained through the use of $|\rho'|$ over the use of $|\rho|$ is shown in Figure 2 as a function of the narrowband interferer carrier frequency ξ normalised to the OFDM sub-carrier spacing $1/(LT)$. Also shown on Figure 2, for reference, are the frequency responses of high pass filters of increasing order and the maximum carrier frequency offset specified by the IEEE 802.11a standard.

This Figure shows, firstly, that the DC offset rejection gained through the use of equation (14) in place of equation (4) is substantial. Secondly, the frequency response of the improvement in narrowband interference rejection gained through the use of equation (14) in place of equation (4) is very similar to that of a first order filter with a cut-off (3 dB) frequency of about $\frac{1}{2}\xi LT$ such as may be implemented, for example, using a coupling capacitor on the input to the analog-to-digital converter. Thirdly, the interference rejection at the maximum expected frequency offset for IEEE 802.11a is less than one decibel. IEEE Standard 802.11a – 1999, Part 11: Wireless LAN Medium Access Control (MAC), and Physical Layer (PHY) Specifications – High-speed Physical Layer in the 5 GHz Band, 1999 is incorporated herein by reference. Referring to the IEEE 802.11a standard, for a maximum input signal level of –30 dBm (17.10.3.4) and a maximum carrier leakage of –15 dBr (17.3.9.6.1), the additional carrier leakage

attenuation required at the receiver to suppress the maximum received carrier level below the minimum receiver sensitivity of -82 dBm (17.3.10.1) is 37 dB. From Figure 2, a tenth order high pass filter does not provide this attenuation across the range of allowable carrier frequency offsets, which means that the only practical reliable method of preventing carrier leakage from producing false detection correlations is accurate time-gating at the transmitter.

Further, a receiver having a dynamic range of 50 dB must be able to suppress narrowband interferers at *any* in-band frequency by at least 50 dB to prevent false detection correlations. Clearly, the use of central correlation alone does not achieve this.

SUMMARY OF INVENTION

It is the object of the invention to provide an OFDM receiver that reduces interference from a narrowband interferer or to at least provide the public with a useful choice.

In broad terms in one aspect the invention comprises a method for reducing interference from at least one narrow band interferer in a pilot symbol assisted OFDM receiver including the steps of; receiving a stream of received data, passing the stream of received data through an adaptive filter that reduces interference from any narrowband interferer, passing the filtered data through a correlator arranged to detect pilot symbols, when a pilot symbol is detected passing the stream of received data to the correlator without first passing the received data through the adaptive filter.

Preferably the number of taps in the adaptive filter is greater than the maximum number of interferers to be cancelled. Ideally the minimum number of taps in the adaptive filter is one greater than the maximum number of interferers to be cancelled.

Preferably the adaptive filter is a normalised least means squares (N-LMS) filter.

Preferably the adaptive filter uses a delayed stream of the received data as a reference signal. Ideally the length of the delay is longer than the length of the pilot symbol.

Preferably the step of detecting a pilot symbol in the correlator includes the steps of detecting a peak in a sliding correlator and when the peak is detected in the sliding correlator operating a matched filter correlator to detect the pilot symbol. In one embodiment the step of detecting a pilot symbol further includes the step of timing out if a pilot symbol is not detected in the matched filter correlator within a predetermined number of matched filter correlator operations.

As a result of frequency offset estimation bias due to a narrowband interferer, the effect of main concern here is on detection methods employing a matched filter. These methods require accurate frequency offset estimation in order to be able to produce the matched filter. Significant frequency estimation bias renders matched filter detection methods ineffective. Further, even if detection is obtained, significant frequency offset estimation bias results in significant frequency offset in the OFDM data, which increases the bit error rate.

In broad terms in another aspect the invention comprises a method for reducing narrowband interference in an OFDM receiver including the steps of receiving a stream of received data, passing the stream of received data through an adaptive filter to reduce interference from any narrowband interferers, passing the output of the adaptive filter to a first correlator, when the first correlator produces a peak over a threshold value triggering a second correlator to search for a pilot symbol in the filtered data, triggering a timeout during which the second correlator will not operate if the second correlator does not detect a pilot symbol in the filtered data without a predetermined number of second correlator operations, and sending a signal that triggers removal of the adaptive filter from the receiver path if the second correlator does detect a pilot symbol in the filtered data within the predetermined number of second correlator operations.

Preferably the first correlator is a sliding window correlator.

Preferably the second correlator is a matched filter correlator.

In broad terms in another aspect the invention comprises a narrowband interference reducing system for an OFDM receiver including a front end arranged to receive data, an adaptive filter arranged to filter narrowband interference from the received data and provide filtered data, a correlator arranged to detect pilot symbols in the filtered data, and a logic system arranged to reroute the received data to the correlator when a pilot symbol has been detected.

It is noted that, at the time of writing, anecdotal evidence suggests a much higher likelihood of interference in the 2.4 GHz ISM band than in the 5 GHz band. The principal immediate application of this invention may be to IEEE 802.11g-compliant WLANs.

The following description concentrates on examining the effect of narrowband interference on the fundamental building block of one L -length PRBS repeated once and with no guard interval or cyclic prefix: the effect on more complicated pilot symbols may be inferred directly from this analysis.

BRIEF DESCRIPTION OF DRAWINGS

The narrowband interference system and method for pilot symbol assisted OFDM receivers of the invention will be further described by way of example only and without intending to be limiting with reference to the following drawings, wherein:

Figure 1A shows the frequency offset estimation bias produced by a single narrowband interferer where the signal to interference ratio is 20dB;

Figure 1B shows the frequency offset estimation bias produced by a single narrowband interferer where the signal to interference ratio is 40dB;

Figure 2 shows the interference rejection where the central correlation coefficient is used as the detection metric;

Figure 3A shows the pilot symbol with one narrowband interferer;

Figure 3B shows the pilot symbol and narrowband interferer after filtering with an N-LMS filter;

Figure 3C shows the change in correlation coefficient over time for the signal of Figure 3A;

Figure 3D shows the change in correlation coefficient over time for the signal of Figure 3B;

Figure 3E is the spectrum of the last 128 samples of the received pilot symbol of Figure 3A;

Figure 3F is the spectrum of the last 128 samples of the received pilot symbol of Figure 3B;

Figure 4A shows the pilot symbol with one narrowband interferer;

Figure 4B shows the pilot symbol and narrowband interferer after filtering with an N-LMS filter;

Figure 4C shows the change in correlation coefficient over time for the signal of Figure 4A;

Figure 4D shows the change in correlation coefficient over time for the signal of Figure 4B;

Figure 4E is the spectrum of the last 128 samples of the received pilot symbol of Figure 4A;

Figure 4F is the spectrum of the last 128 samples of the received pilot symbol of Figure 4B;

Figure 5A shows the pilot symbol with one narrowband interferer;

Figure 5B shows the pilot symbol and narrowband interferer after filtering with an N-LMS filter;

Figure 5C shows the change in correlation coefficient over time for the signal of Figure 5A;

Figure 5D shows the change in correlation coefficient over time for the signal of Figure 5B;

Figure 5E is the spectrum of the last 128 samples of the received pilot symbol of Figure 5A;

Figure 5F is the spectrum of the last 128 samples of the received pilot symbol of Figure 5B;

Figure 6A shows the pilot symbol with one narrowband interferer;

Figure 6B shows the pilot symbol and narrowband interferer after filtering with an N-LMS filter;

Figure 6C shows the change in correlation coefficient over time for the signal of Figure 6A;

Figure 6D shows the change in correlation coefficient over time for the signal of Figure 6B;

Figure 6E is the spectrum of the last 128 samples of the received pilot symbol of Figure 6A;

Figure 6F is the spectrum of the last 128 samples of the received pilot symbol of Figure 6B;

Figure 7A shows the pilot symbol with two narrowband interferers;

Figure 7B shows the pilot symbol and narrowband interferers after filtering with an N-LMS filter;

Figure 7C shows the change in correlation coefficient over time for the signal of Figure 7A;

Figure 7D shows the change in correlation coefficient over time for the signal of Figure 7B;

Figure 7E is the spectrum of the last 128 samples of the received pilot symbol of Figure 7A;

Figure 7F is the spectrum of the last 128 samples of the received pilot symbol of Figure 7B;

Figure 8A shows the pilot symbol with two narrowband interferers;

Figure 8B shows the pilot symbol and narrowband interferers after filtering with an N-LMS filter;

Figure 8C shows the change in correlation coefficient over time for the signal of Figure 8A;

Figure 8D shows the change in correlation coefficient over time for the signal of Figure 8B;

Figure 8E is the spectrum of the last 128 samples of the received pilot symbol of Figure 8A;

Figure 8F is the spectrum of the last 128 samples of the received pilot symbol of Figure 8B;

Figure 9A shows the pilot symbol with one narrowband interferer;

Figure 9B shows the pilot symbol and narrowband interferer after filtering with an N-LMS filter;

Figure 9C shows the change in correlation coefficient over time for the signal of Figure 9A;

Figure 9D shows the change in correlation coefficient over time for the signal of Figure 9B;

Figure 9E is the matched filter correlation function of the received pilot symbol of Figure 9A;

Figure 9F is the matched filter correlation function of the received pilot symbol of Figure 9B;

Figure 10A is a block diagram showing the N-LMS filter in the front end of the receiver chain; and

Figure 10B is a flow chart showing the interactions between the two-stage detection process and the N-LMS filter.

DETAILED DESCRIPTION

Effective narrowband interference suppression is required to improve the reliability of pilot-symbol assisted detection in OFDM systems. Adaptive filters can be used to provide interference suppression. One type of adaptive filter the normalised least mean squares (N-LMS) algorithm is able to be applied to suppress narrowband interference, as follows.

An M length finite impulse response (FIR) having a time-varying coefficient vector $\mathbf{w}_m \triangleq [w_m, w_{m+1}, \dots, w_{m+M-1}]^T$ is innovated using the update equation

$$\mathbf{w}_{m+1} = \mathbf{w}_m + \frac{\mu}{\delta_\mu + \|\mathbf{u}_m\|^2} \mathbf{u}_m e_m^*, \quad (18)$$

where \mathbf{u}_m is a sample vector of reference signal, μ is an adaptation coefficient, δ_μ is a small positive constant, $\|\cdot\|$ denotes the Euclidean norm and

$$e_m = r_m - y_m \quad (19)$$

is the system output and estimation error for filter output

$$y_m = \mathbf{w}_m^H \mathbf{u}_m, \quad (20)$$

noting that r_m , as described previously, is the m th sample of receiver (baseband) input.

Ideally, the reference signal comprises interference, which is correlated with the interference in the input signal, and desired signal and noise which are uncorrelated with desired signal and noise in the input signal. One way to achieve this is to produce the reference signal as a time-lagged version of the input signal, such that $\mathbf{u}_m = \mathbf{r}_{m+K}$ for lag K and where K is chosen to be larger than the length of the pilot symbol.

This implementation of the LMS algorithm is capable of robustly suppressing multiple narrowband interferers. A useful rule of thumb is that an M coefficient N-LMS filter can suppress $M-1$ narrowband interferers. Table 1 shows the computational complexity of the normalised least mean squares (N-LMS) algorithm for an M -tap filter compared to that of the LMS algorithm. The estimated total number of cycles assumes that six cycles are required to implement each division. Note that, although the N-LMS is more than thrice as computationally expensive as the LMS, the additional robustness provided by the N-LMS to gradient noise amplification more than justifies the additional complexity.

Table 1

	M Taps	$M=3$		$M=4$	
N-LMS	18M+4MULT	58	MULT	76	MULT
	13M+4ADD	43	ADD	56	ADD
	2M DIV	6	DIV	8	DIV
	30M+4 Cycles	94	Cycles	124	Cycles
LMS	8M+4 MULT	28	MULT	36	MULT
	8M+2 ADD	26	ADD	34	ADD
	8M+4 Cycles	28	Cycles	36	Cycles

EXAMPLES

Pilot symbol detection in the presence of narrowband interference was simulated to confirm the efficacy of interference cancellation based on the N-LMS algorithm and to identify implementation issues associated with a practical receiver.

To demonstrate the effect of narrowband interference on pilot symbol based receivers, and to establish the efficacy of the N-LMS algorithm in suppressing the effects of narrowband interference, the following simulation was performed. The IEEE 802.11a long pilot symbol was transmitted, both preceded and succeeded by AWGN. One or more narrowband interferers were added to the transmitted signal. One receiver chain had no interference suppression and performed pilot symbol based detection by calculating the non-central correlation function of equation (4) and the central correlation function of equation (14). The second receiver chain performed the N-LMS algorithm at the input, followed by pilot symbol detection using the non-central correlation function of equation (4). IEEE 802.11a system parameters were used, so the length of one PRBS in the pilot symbol $L=64$ and $T=50$ ns. For all simulations, the number of N-LMS filter taps used was $M=3$, the lag (delay) between the primary input and the reference input was $K(=4 \times L)=256$ taps, the adaptation coefficient $\mu=0.1$ and constant $\delta_\mu=0.0001$. These simulations assume an ideal implementation with no carrier frequency or phase offset and no sample timing offset.

As will be seen in the examples there is a need to remove the adaptive filter from the receiver path once a pilot symbol has been detected. One method for determining when to remove the N-LMS filter from the receiver chain requires a two-stage detection process. The output from the sliding window correlator is compared to a threshold of detection, set at a level to minimise the probability of false detection while also minimising the probability of missed detection, as described in A.J. Coulson, "Maximum Likelihood Synchronization for OFDM Using a Pilot Symbol: Analysis", IEEE J. Selected Areas in Communications, vol. 19, no.12, pp 2495 – 2503, December 2001. Once this threshold has been exceeded a second, matched filter, detector is enabled. The matched filter detector, although computationally expensive, is exercised

only for a few sample periods and produces excellent localisation and interference immunity. For application to interference suppression, the matched filter "peak" can be used to determine when to switch the N-LMS filter out of the receiver chain.

A block diagram of this interference suppression system is shown in Figure 10A, and a flowchart outlining its operation is shown in Figure 10B. The N-LMS filter comprises blocks 2, 3 and 4 between Front End 1 and switches 5 and 6. Block 2 is a K element delay where K is an integer number of symbol periods larger than the length of the pilot symbol. As shown in Figure 10A when switches 5 and 6 are in the position shown (closed and open respectively) the N-LMS filter is switched into the receiver. In this position the output of the N-LMS filter passes to sliding correlator 7 and matched filter correlator 8. The logic level output of the sliding window correlator enables the matched filter detector when the threshold of correlation is exceeded. This may occur for two reasons.

1. A narrowband interferer can "appear", and will produce high correlation from the sliding window correlator while the N-LMS filter adapts to suppress the interferer. This can be seen at the start of Figures 3D, 4D, 5D, 6D, 7D and 8D. In this case, the correlator logic output enables the matched filter detector by setting logic operator D1 to 1, but the matched filter detector will not produce a correlation peak, as there is no pilot symbol present. A state machine is provided to disable the matched filter detector after a certain number of input samples (or matched filter correlation operations) have been processed. This is shown in Figure 10B. In Figure 10B once detection is started the state machine flows in a loop asking whether the sliding correlator has reached a threshold value. This is shown in box 12 where the question is asked has the logic output of the sliding correlator been set. The logic output of the sliding correlator is set when the sliding correlator reaches a threshold value.

Once the logic output of the sliding correlator has been set the matched filter is operated. The matched filter correlator will exceed a threshold value if a pilot symbol is present. If the threshold is exceeded the logic operator D2 is set. Question

box 14 queries whether logic operator D2 is set. If logic operator D2 is not set question box 15 queries whether the counter has exceeded a preset value (for example 10). If the counter has not exceeded the preset value the counter is incremented in box 17 and the question is again asked whether logic operator D2 is set. If the counter has exceeded the preset value the yes arrow is followed from question box 15 to box 17 where a timeout is begun.

At timeout box 17 the state machine assesses that a false correlation has occurred, disables the matched filter detector and ignores the sliding window correlator output for a "timeout period", set to be longer than the adaptation time of the N-LMS filter, say up to 1000 input sample periods. After the "timeout period" the state machine resets to the initial state and begins to query whether the sliding correlator logic operator is set.

2. A pilot symbol appears, producing a correlation peak from the sliding window correlator. Again this is shown at box 12 of Figure 10B where when the sliding correlator produces a peak, logic operator D1 is set. The logic output of the sliding window correlator enables the matched filter detector, which will produce a correlation peak after a small number of input samples, typically five. In this operation the state machine is at box 14 where a query is run asking whether the matched filter correlator has produced a peak. The matched filter correlator produces a peak and exceeds the threshold value. This then sets logic operator D2. When operator D2 is set (before the counter is exceeded) the yes arrow is followed from box 14 to box 18 and the N-LMS filter is switched out of the receiver path. The logic output of the matched filter detector acts to remove the N-LMS filter from the receiver chain by reversing the polarity of each of the two switches 5 and 6 shown in Figure 10A.

In this way the problem of a false packet detect caused by the N-LMS filter adapting to the interferer and the problem of ISI caused by the N-LMS filter are overcome.

The second implementation issue is the spectral leakage, produced by large interferers, causing intercarrier interference. Simple search techniques on the pilot symbol data spectrum (FFT) will enable identification of the interference-affected bins, and appropriate measures then can be applied to post-pilot-symbol OFDM data. This can be aided by the N-LMS filter at the front end, which provides both signal-plus-noise and interference-plus-noise signals which may be used, in conjunction with the pilot symbol itself, to estimate SNR and SIR per packet.

It should be noted that interference suppression using N-LMS filter can be expected to perform equally well in either a frequency non-selective or a frequency-selective environment, as there is no assumption of desired signal spectral characteristic either explicit or implicit in the formulation of the N-LMS algorithm. It was found empirically in producing the results in the examples that an M tap N-LMS filter can be expected to perform well in suppressing $M-1$ narrowband interferers. The value $M=3$ was chosen to be able to suppress two narrowband interferers, such as may be expected from an analog cordless telephone handset and base pair. Finally, the N-LMS algorithm, being adaptive, can be expected to perform well where slow time-variation occurs either in the channel and or in the narrowband interferer signal or both.

Example 1

Figure 3 shows results for a signal to noise ratio (SNR) of 20 dB and a signal to interferer ratio (SIR) of 15 dB. Figure 3A shows the real part of the (unfiltered) input to the pilot symbol correlator of the first receiver, while Figure 3B shows the real part of the output from the N-LMS filter at the input to the pilot symbol correlator of the second receiver. It can be seen that the magnitude of the first $74\mu\text{s}$ of the unfiltered signal (shown in Figure 3A) is slightly greater than that for the N-LMS filtered signal (shown in Figure 3B), and that the portion of both input signals containing the pilot symbol (which occupies the next $8\mu\text{s}$) has a magnitude which is much larger than that of the interference plus noise signal.

Figure 3C shows the central and non-central correlation functions evaluated in the first receiver, showing that both produce high correlation for the entire time series. The

correlation for the first $74\mu\text{s}$ represents the correlation of a narrowband interferer in AWGN, whereas correlation for the next $14\mu\text{s}$ represents the correlation of a pilot symbol in interference plus AWGN. It can be seen from Figure 3C that pilot symbol detection based on sliding window correlation alone is problematic in the presence of a narrowband interferer, irrespective of whether the non-central or central correlation function is used.

Figure 3D demonstrates that the N-LMS filter has a dramatic effect on the correlation function, which appears very similar to the interference-free case. The effect of producing the N-LMS reference signal from a delayed input clearly can be seen in Figure 3D, also. The reference signal produces a significant correlation output at around $95\mu\text{s}$, which is due to the pilot symbol feeding through the N-LMS filter on the reference signal.

Using the interference suppression system of Figures 10A and 10B when the correlation peak at about $80\mu\text{s}$ occurs the sliding correlator activates the matched filter receiver. The matched filter receiver detects a pilot symbol and sends out a signal that results in the adaptive filter being switched out of the receiver path before the second correlation peak at about $95\mu\text{s}$ occurs. Using the adaptive filter and logic system with the sliding correlator and matched filter correlator the narrowband interferer is suppressed and the pilot symbol correctly identified in this example.

The spectra of the signals at the input to the correlators are shown in Figure 3E, for the unfiltered case, and Figure 3F, for the N-LMS filtered case. The spectra were produced from the last 128 (which is $2 \times L$) samples of the pilot symbol input into the correlators. The narrowband interferer is clearly visible at around 4 MHz in the unfiltered signal of Figure 3E, and the effect of the N-LMS filter on the pilot symbol spectrum can be seen by examining the same part of the spectrum in Figure 3F. These spectra show that, with an SIR of 15 dB, the interferer magnitude is about the same as the magnitude of the affected pilot symbol sub-carrier: this may be regarded as fairly modest interference.

Example 2

The effect of more severe interference can be seen in Figure 4, for a single interferer with SNR of 20 dB and SIR of 0 dB. Figure 4A shows the real part of the (unfiltered) input to the pilot symbol correlator of the receiver, while Figure 4B shows the real part of the output from the N-LMS filter at the input to the pilot symbol correlator of the second receiver. It can be seen that the magnitude of the first $74\mu\text{s}$ of the unfiltered signal is much greater than that for the N-LMS filtered signal, and that the portion of both input signals containing the pilot symbol (which occupies the next $8\mu\text{s}$) has a magnitude that is larger than that of interference plus signal noise. Figure 4B shows that the N-LMS filter reduces the interference at the correlator input.

Figure 4C shows the central and non-central correlation functions evaluated in the first receiver, showing that both produce high correlation for entire time series except immediately following reception of the actual pilot symbol. The correlator outputs in the unfiltered receiver can be seen from Figure 4C to be of no value in detecting the pilot symbol for this amount of interference.

Figure 4D shows that the resulting correlator output produces a correlation peak very similar to that expected in an interference-free environment. Again the effect of producing the N-LMS reference signal from a delayed input can clearly be seen in Figure 4D. The reference signal produces a significant correlation output at around $95\mu\text{s}$, which is due to the pilot symbol feeding through the N-LMS filter on the reference signal.

As shown in Figure 4D the sliding window correlator initially produces an output that exceeds the threshold value. At this point the matched filter correlator is started. The matched filter correlator searches for a pilot symbol. Using the interference suppression system of Figures 10A and 10B in each stage of the matched filter detection a counter is incremented. As there is no pilot symbol at the start of the received data the matched filter counter will exceed a predetermined value before a pilot symbol is detected. The matched filter will go into timeout mode for a predetermined period following which the sliding window correlator will resume searching for a pilot symbol. The sliding window correlator will detect the pilot symbol at about $80\mu\text{s}$ and start the matched filter

correlator again. The matched filter correlator then determines that there is a pilot symbol and sends out a signal that results in the adaptive filter being switched out of the receiver path before the second correlation peak at about 95 μs occurs. In this example the initial correlation peak detected by the sliding window correlator while it is adapting to the narrowband interferer is rejected by the interference suppression system as not containing a pilot symbol. When the pilot symbol is detected the adaptive filter is switched out of the receiver path before it can cause a false peak in the sliding window correlator. Note that in Figure 4D if the adaptive filter remains in place, as is shown in this Figure, the second false correlation peak (at 95 μs) will not trigger the matched filter correlator as it is not larger than the threshold value.

Of additional interest is the unfiltered signal spectrum of Figure 4E, showing "spectral leakage" from the interferer into adjacent frequency bins. This is due to the interferer not having an integral number of carrier periods in the OFDM symbol period. Figure 4F shows that the magnitude of the interferer has been reduced by using the N-LMS filter.

Example 3

Figure 5 shows an example having a single interferer with large SNR, 40 dB, and large SIR, 30 dB. Figure 5A shows the real part of the (unfiltered) input to the pilot symbol correlator of the first receiver while Figure 5B shows the real part of the output from the N-LMS filter at the input to the pilot symbol correlator of the second receiver. It can be seen that the magnitude of the first 74 μs of the unfiltered signal is greater than that for the N-LMS filtered signal, and that the portion of both input signals containing the pilot symbol (which occupies the next 8 μs) has a magnitude which is much larger than that of the interference signal plus noise signal.

Figure 5C shows central and non-central correlation functions evaluated at the first receiver. As can be seen in Figure 5C both correlators produce a high output when the interferer is present with no pilot symbol leading to a false packet detect. Figure 3C demonstrates that interference-only correlation (as shown in the first 74 μs of this figure)

is a function of interference-to-noise ratio alone, and that even signals having high SNR are problematic to detect in the presence of a much lower power interferer.

Figure 5D shows the correlation when the incoming data is filtered by the N-LMS filter. Again the correlation function of the filtered data is very similar to that expected when no interferer is present. Figures 5E and 5F are spectra of the unfiltered and filtered signals respectively.

As shown in Figure 5D the sliding window correlator initially produces an output that may exceed the threshold value depending on where the threshold value is set. If the threshold value is exceeded the matched filter correlator is started. The matched filter correlator searches for a pilot symbol. Using the interference suppression system of Figures 10A and 10B in each stage of the matched filter detection a counter is incremented. As there is no pilot symbol at the start of the received data the matched filter counter will exceed a predetermined value before a pilot symbol is detected. The matched filter will go into timeout mode for a predetermined period following which the sliding window correlator will resume searching for a pilot symbol. The sliding window correlator will detect the pilot symbol at about 80 μ s and start the matched filter correlator again. The matched filter correlator then determines that there is a pilot symbol and sends out a signal that results in the adaptive filter being switched out of the receiver path before the second correlation peak at about 95 μ s occurs. In this example the initial correlation peak detected by the sliding window correlator while it is adapting to the narrowband interferer is rejected by the interference suppression system as not containing a pilot symbol. When the pilot symbol is detected the adaptive filter is switched out of the receiver path before it can cause a false peak in the sliding window correlator. Note that in Figure 5D if the adaptive filter remains in place as is shown in this Figure the second false correlation peak (at 95 μ s) is probably not larger than the threshold value so will not trigger the matched filter correlator.

Example 4

Figure 6 shows an example having a signal interferer with SNR=20 dB, SIR= 15 dB and the interferer (demodulated) carrier frequency being close to DC. This situation can occur as a result of carrier feedthrough at the transmitter.

Figure 6A shows the unfiltered received signal and Figure 6B shows the received signal after being filtered with an N-LMS filter.

Figure 6C shows the central and non-central correlation functions applied to the unfiltered data. This figure shows that, in this case, the central correlation function, ρ_c (from equation 14), produces a lower correlation value than the non-central correlation function, ρ_n (from equation 4). The normalised carrier frequency in this example is $\xi_{LT}=0.32$ which is expected, from the theoretical development the background section and the result shown in Figure 2, to produce a correlation attenuation of about 6 dB from using the central correlation function compared with the non-central correlation function. Casual inspection of Figure 6C indicates that the simulation confirms this expectation. Note that the maximum normalised carrier offset (maximum carrier frequency expected as a result of carrier feedthrough) permitted by IEEE 802.11a is $\xi_{LT}=0.67$.

Figure 6D shows that the N-LMS filtered receiver results in better interference suppression than the unfiltered receiver employing either the central or the non-central correlation function. Again Figures 6E and 6F show the unfiltered and N-LMS filtered spectra respectively.

As can be seen in Figure 6D there is an initial peak in the output of the sliding correlator as the adaptive filter adjusts and begins to filter out the narrowband interferer. Depending on where the threshold value is set this initial peak may or may not trigger the matched filter. Using the interference suppression system of Figures 10A and 10B if the matched filter is triggered it will set the timeout after the predetermined number of counts has been met as there is no pilot symbol. The pilot symbol will be correctly detected when it begins. In this example the false correlation peak at 95 μ s is much

lower than the threshold value so if the adaptive filter were left in place this would not trigger the matched filter correlator.

Example 5

Figure 7 shows an example of two narrowband interferers, where the SNR is 20 dB and the SIRs are 10.4 dB and 9.5 dB for the two interferers.

Figure 7A shows the unfiltered signal and Figure 7B shows the signal after passing through an N-LMS filter. As can be seen the signal before the pilot symbol begins is reduced in Figure 7B.

Figure 7C shows the central and non-central correlation functions for the unfiltered signal. With the threshold set to 0.8, using either the central or the non-central correlation function will produce a false start of packet before the pilot symbol is detected. Figure 7D shows that the N-LMS filter suppresses the two interferers to the extent that the pilot symbol correlation detection output closely resembles the interferer-free case.

As can be seen in Figure 7D there is an initial peak in the output of the sliding correlator as the adaptive filter adjusts and begins to filter out the narrowband interferers. Depending on where the threshold value is set this initial peak may or may not trigger the matched filter. If the matched filter is triggered it will set the timeout after the predetermined number of counts has been met as there is no pilot symbol. The pilot symbol will be correctly detected when it begins. In this example the false correlation peak at 95 μ s is much lower than the threshold value and if the adaptive filter were left in place this would not trigger the matched filter correlator.

Figures 7E and 7F show the unfiltered and N-LMS filtered spectra respectively. In particular the interferers can be seen in Figure 7E at about 3MHz and 7MHz. These interferers have both been reduced in the spectrum of Figure 7F.

Example 6

Figure 8 shows a second example of two narrowband interferers, where the SNR is 20 dB and the SIRs are -20 dB and -10 dB for the two interferers.

Figure 8A shows the received signal. This Figure shows that these high power interferers completely “swamp” the unfiltered receiver. Figure 8B shows the received signal after passing through an N-LMS filter.

Figure 8C shows the central and non-central correlation functions for the unfiltered signal. This figure shows that the high power interferers completely swamp the unfiltered receiver. Figure 8D shows the correlation function of the N-LMS filtered data. This figure shows that the N-LMS filtered receiver chain takes much longer to adapt and suppress the interferers in this example than in previous examples. This is due to the power differential between the two interferers, leading to the correlation matrix having widely spread eigenvalues, which means that the lower power interferer is “masked” until the higher power interferer is sufficiently suppressed. Nonetheless, the N-LMS filter suppresses the interferers to the extent that robust correlation detection can be seen in Figure 8D. This figure also highlights that, as in Figures 3-7, the delayed (reference) input to the N-LMS algorithm re-injects the pilot symbol into the received signal after the K tap delay. Furthermore, in a high power interferer environment, the reference signal copy of the pilot symbol is of similar magnitude to the primary signal copy. In an OFDM packet, this will have the effect of introducing significant inter-symbol interference into the OFDM data stream.


As can be seen in Figure 8D there is an initial peak in the output of the sliding correlator as the adaptive filter adjusts and begins to filter out the narrowband interferers. Using the interference suppression system of Figures 10A and 10B the initial peak triggers the matched filter. The matched filter sets the timeout after the predetermined number of counts has been met as there is no pilot symbol. Following the timeout period the sliding window correlator will again detect a pilot symbol due to the second narrowband interferer. Again the matched filter will be triggered and will again timeout when a pilot symbol is not detected by the matched filter. The pilot symbol will be correctly

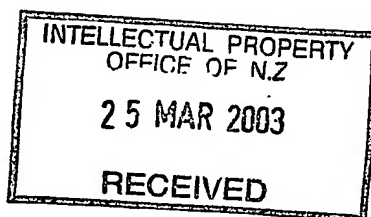
detected when it begins at 75 μ s. Once the pilot symbol is detected the adaptive filter is removed from the receiver path so that the correlation peak that would be caused by the adaptive filter at 95 μ s is not present. After the adaptive filter has been removed from the receiver path normal channel estimation process can be augmented also to estimate the interferer(s), and previously proposed equalization techniques for OFDM data can be applied.

Figures 8E and 8F show the spectra of the unfiltered and filtered data respectively. Note that, in this example, the time domain data was windowed (using a Kaiser window with $\beta=6$) prior to performing the FFT used to produce the spectra of Figures 8E and 8F. This was done to reduce the spectral leakage, mentioned above, which otherwise almost completely obscures the pilot symbol data in the unfiltered signal spectrum shown in Figure 8E.

The operation of the matched filter is shown in Figure 9, where both the unfiltered receiver and the N-LMS filter receiver can be seen to produce distinct matched filter peaks in Figures 9E and 9F, respectively. The initial peak of about 0.5 is produced by the cyclic prefix in the IEEE 802.11a long pilot symbol. The first large peak is produced by the first copy of the PRBS, and the second large peak is produced by the second copy of the PRBS in the pilot symbol. In this example, which is produced by a simulation running in non real time, the matched filter detector is exercised continuously for all data input into the receiver. In a practical receiver, the matcher filter will be enabled by a state machine triggered by the sliding window detector output exceeding the correlation threshold. In this way, the matched filter would be run, in this example, for a few samples at around 80 μ s, that is, in the vicinity of the second (large) matched filter detector peak. At the point where the matched filter detector output exceeds the correlation threshold (at the second large peak) the N-LMS filter is switched out of the receiver chain — thus preventing the delayed pilot symbol (in the N-LMS filter reference channel) from appearing in subsequent OFDM data and causing intersymbol interference.

The foregoing describes the invention including preferred forms thereof. Alterations and modifications as will be obvious to those skilled in the art are intended to be incorporated in the scope hereof.

Industrial Research Limited
By the authorised agents
A. J. PARK
Per 



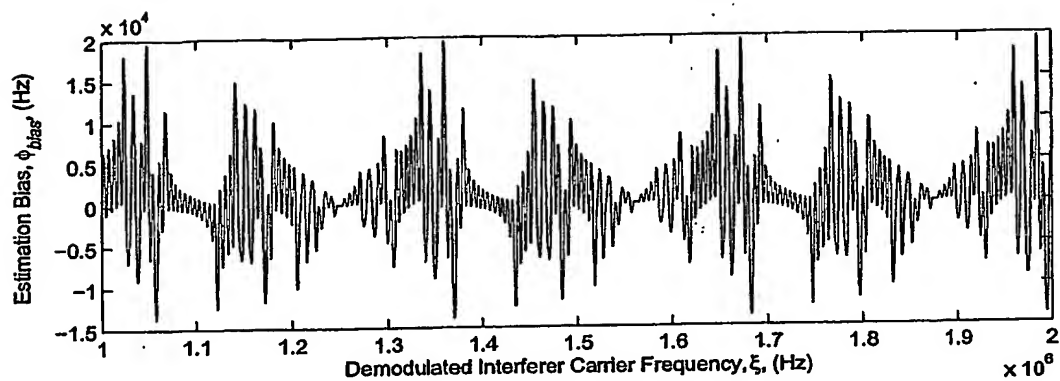


Figure 1A

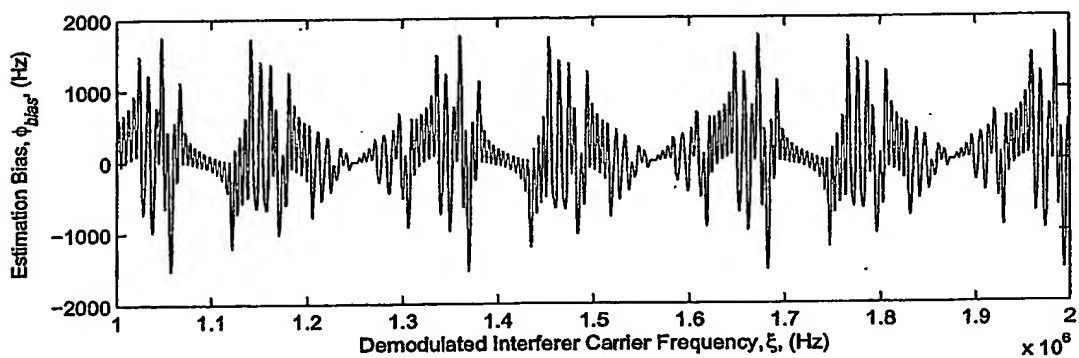


Figure 1B

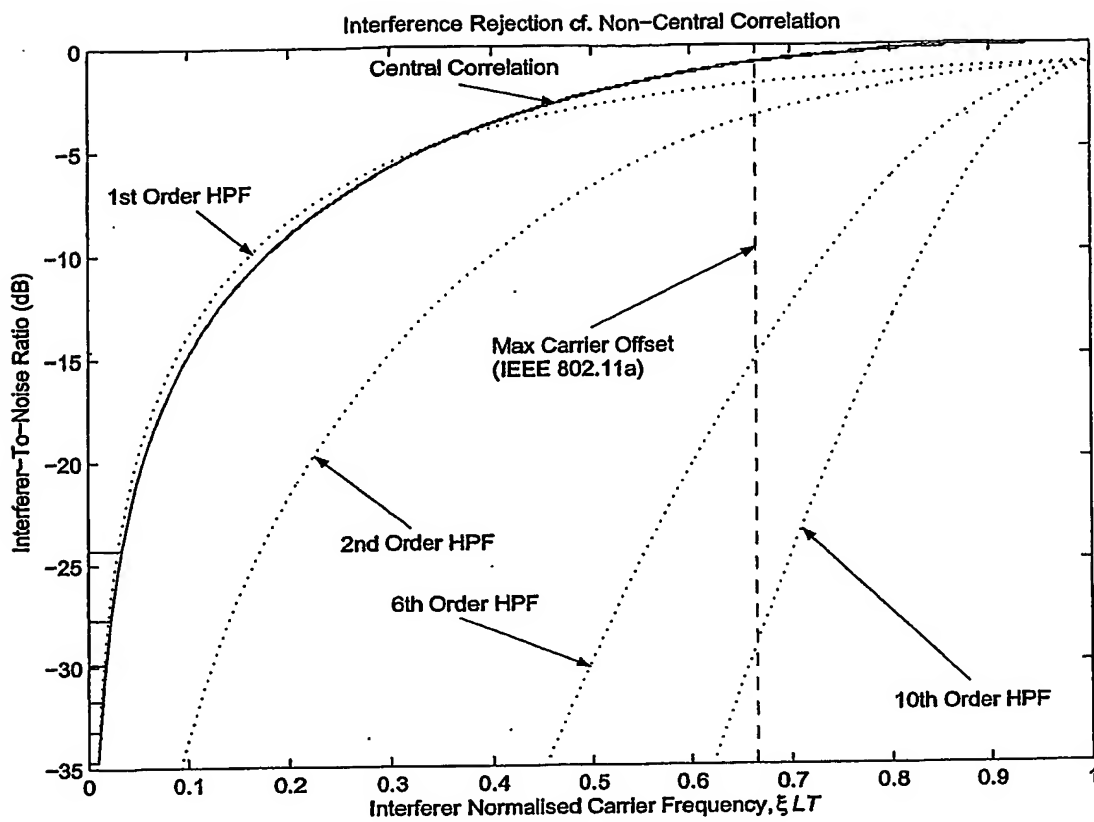


Figure 2

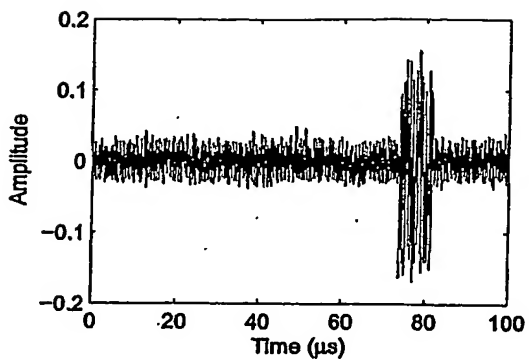


Figure 3A

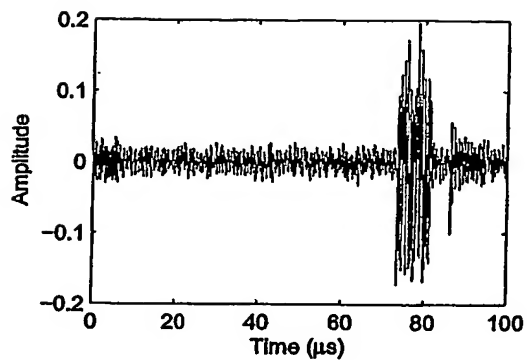


Figure 3B

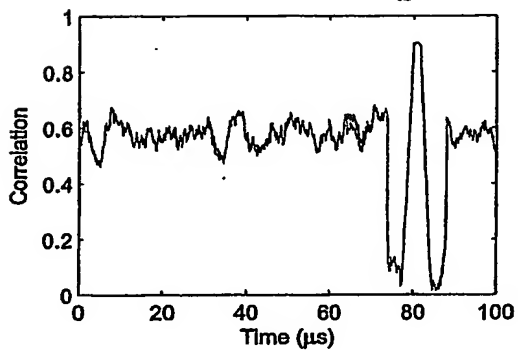


Figure 3C

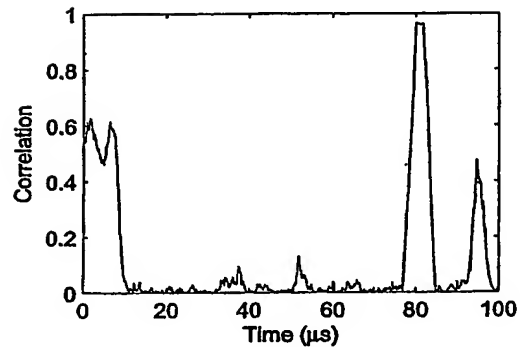


Figure 3D

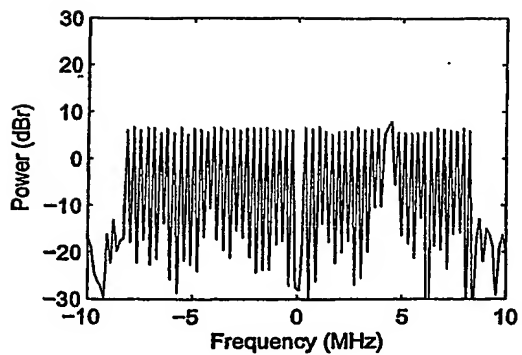


Figure 3E

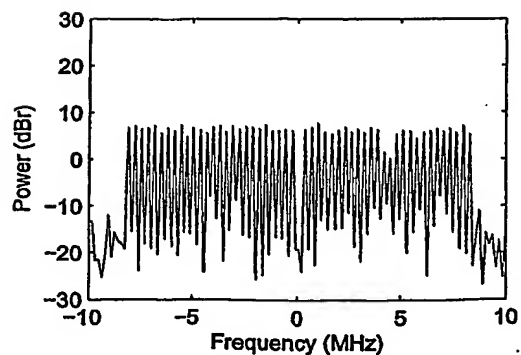


Figure 3F

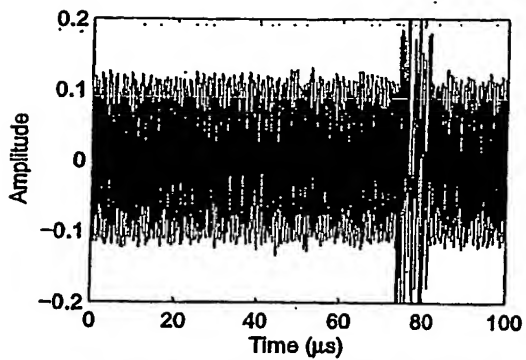


Figure 4A

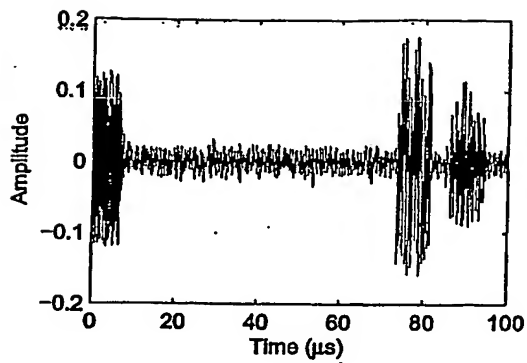


Figure 4B

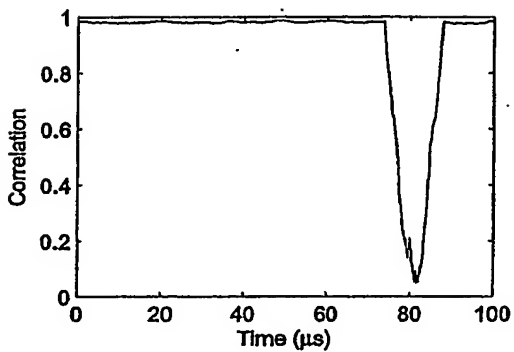


Figure 4C

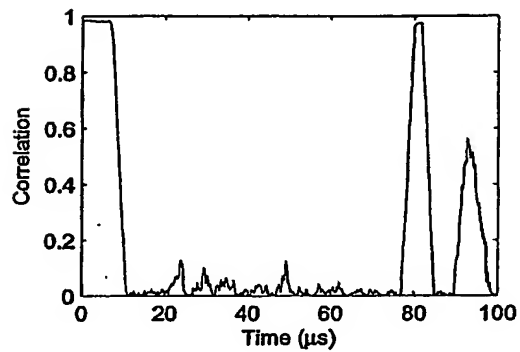


Figure 4D

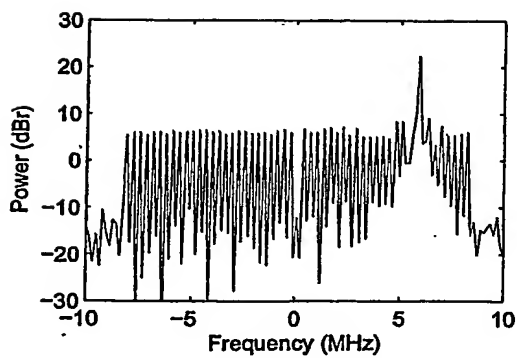


Figure 4E

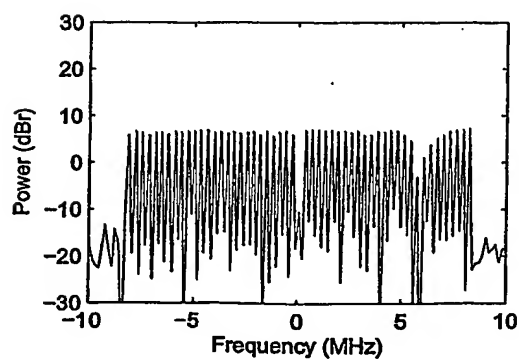


Figure 4F

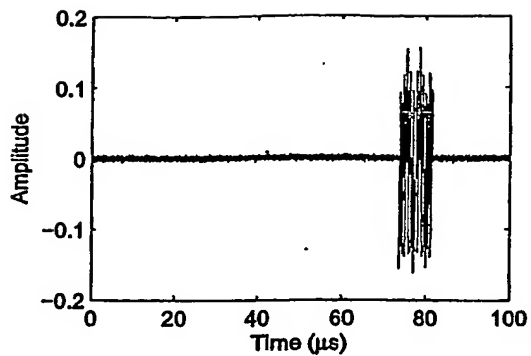


Figure 5A

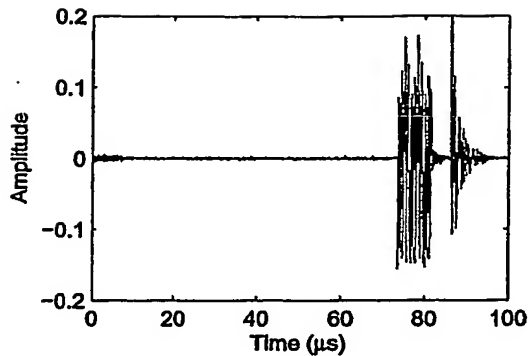


Figure 5B

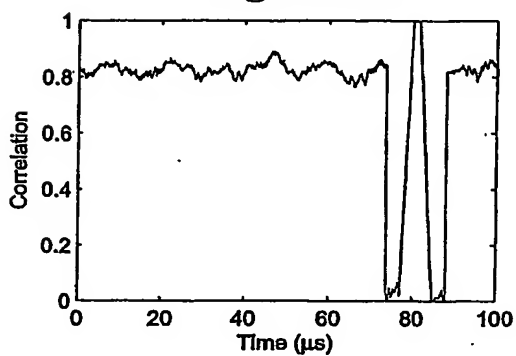


Figure 5C

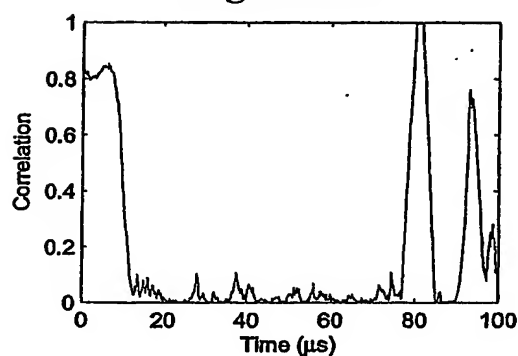


Figure 5D

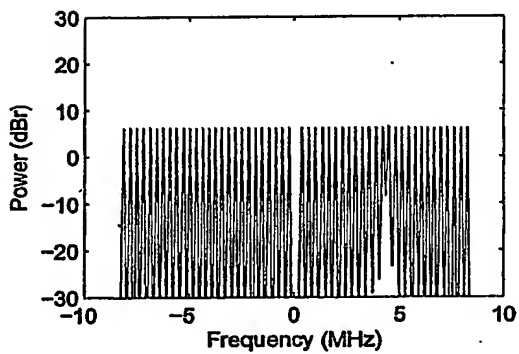


Figure 5E

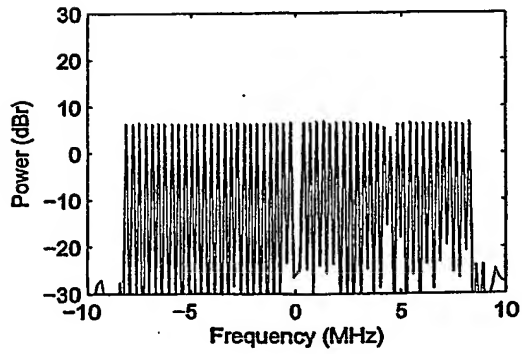


Figure 5F

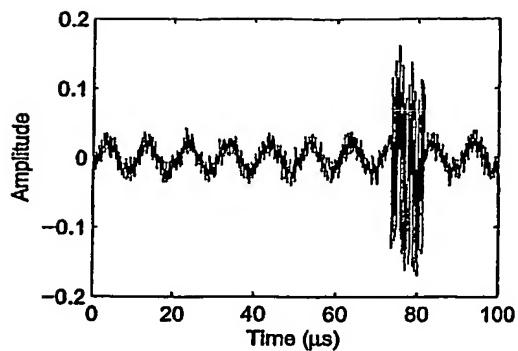


Figure 6A

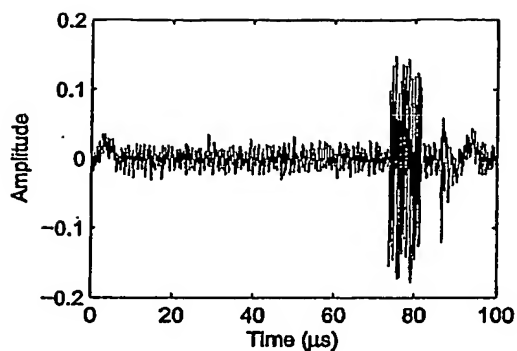


Figure 6B

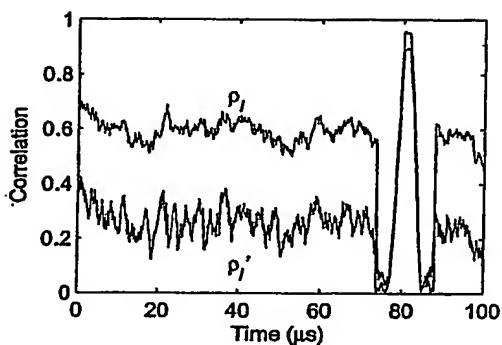


Figure 6C

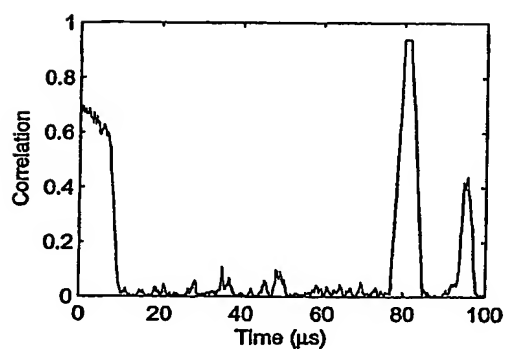


Figure 6D

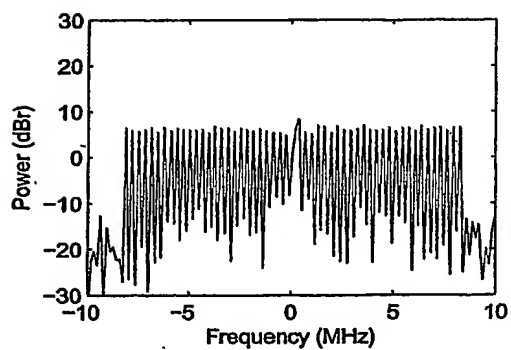


Figure 6E

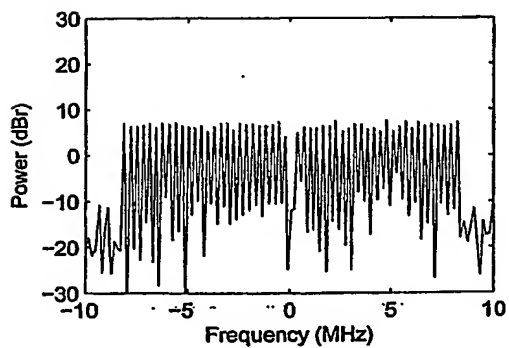


Figure 6F

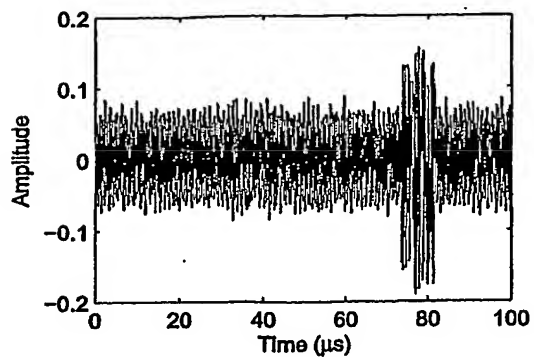


Figure 7A

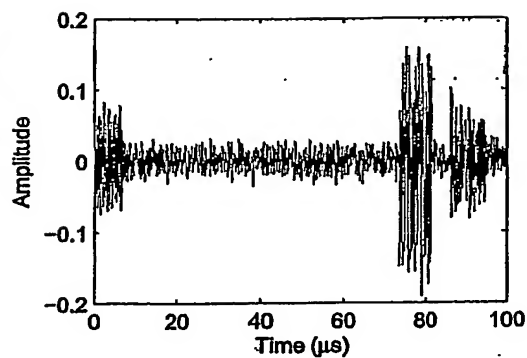


Figure 7B

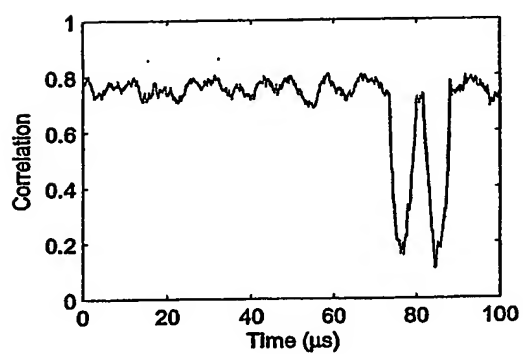


Figure 7C

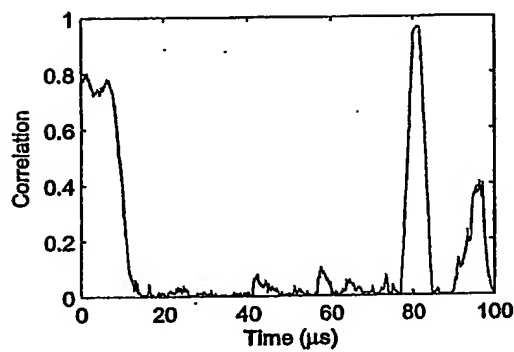


Figure 7D

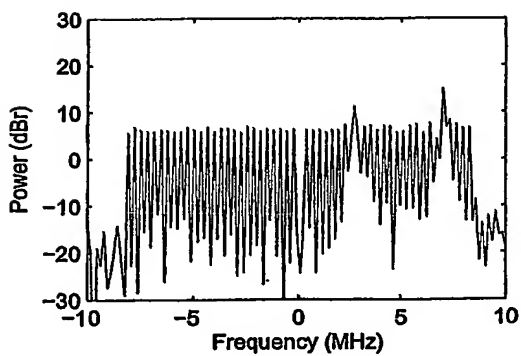


Figure 7E

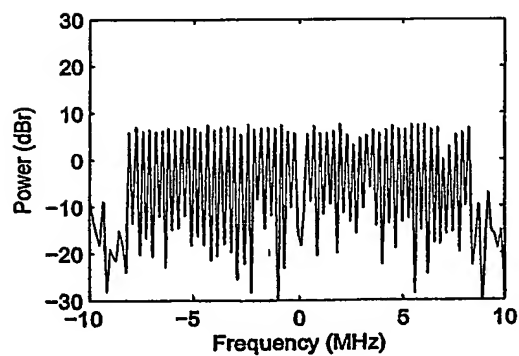


Figure 7F

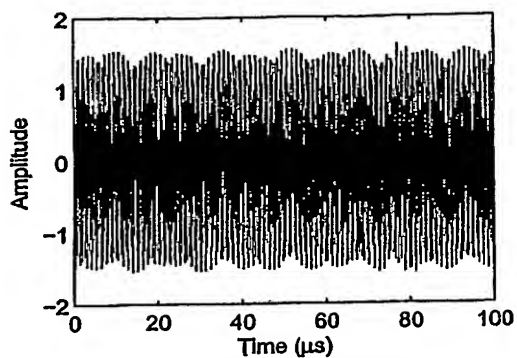


Figure 8A

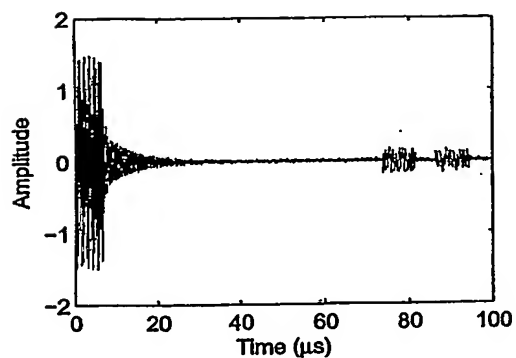


Figure 8B

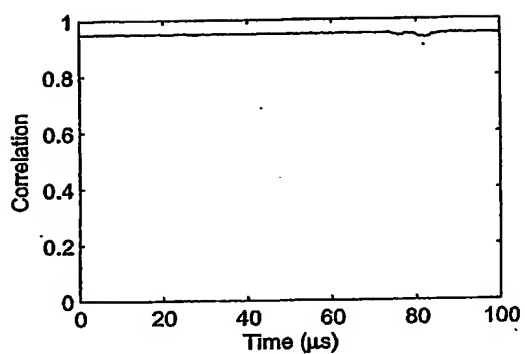


Figure 8C

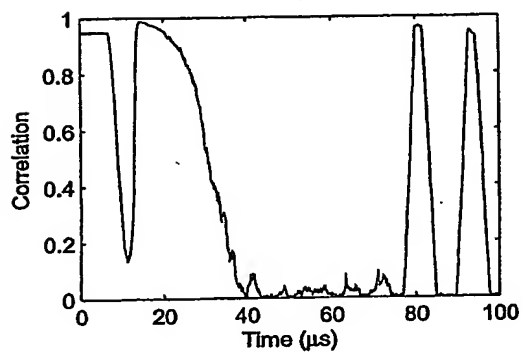


Figure 8D

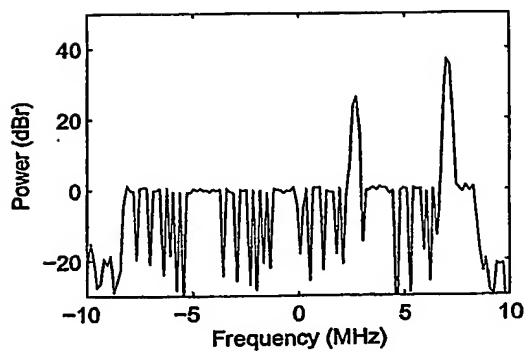


Figure 8E

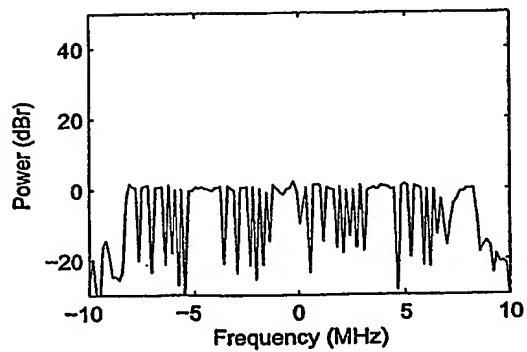


Figure 8F

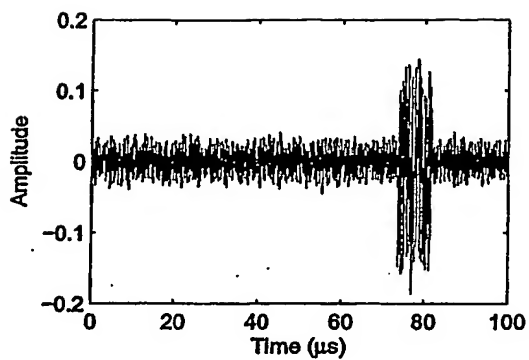


Figure 9A

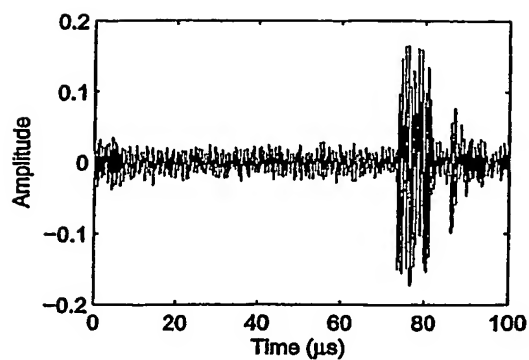


Figure 9B

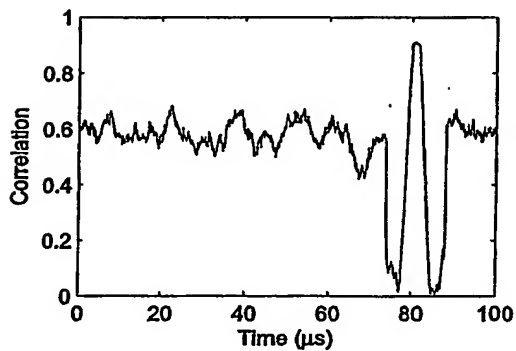


Figure 9C

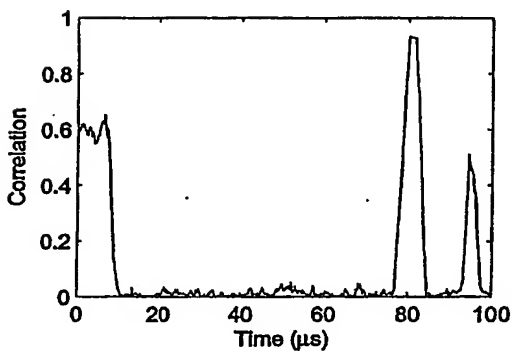


Figure 9D

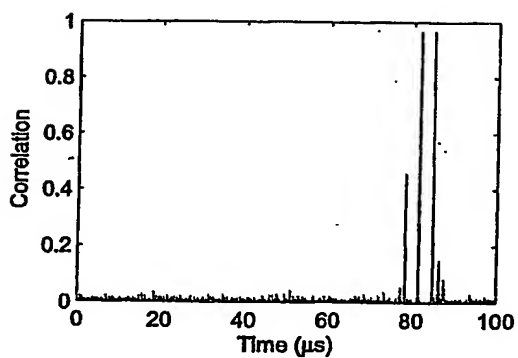


Figure 9E

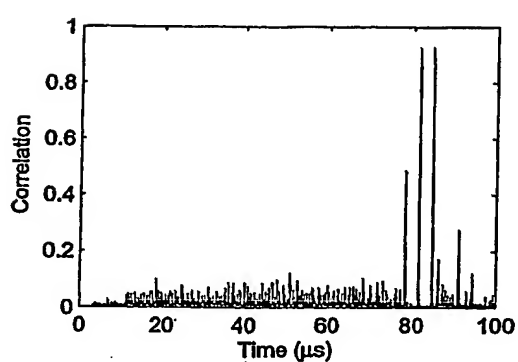


Figure 9F

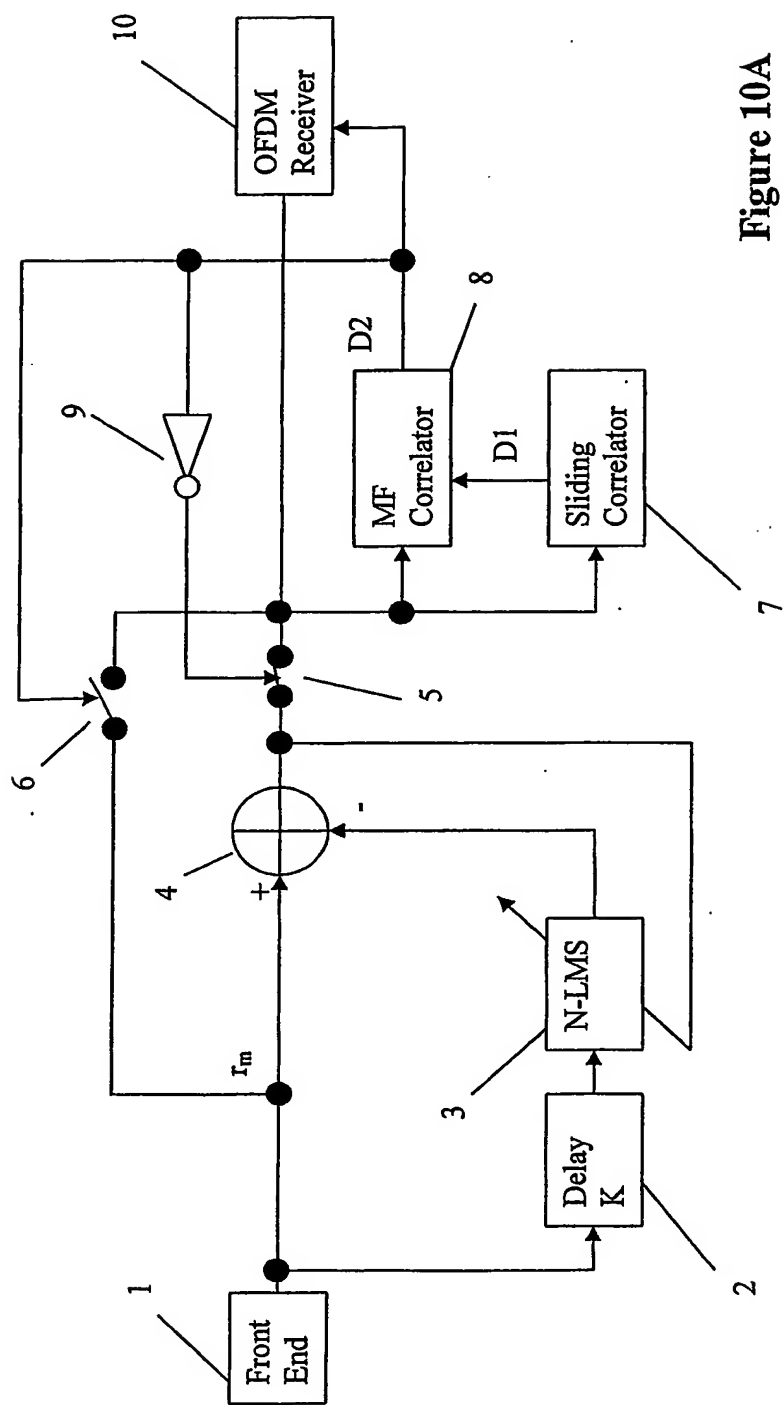


Figure 10A

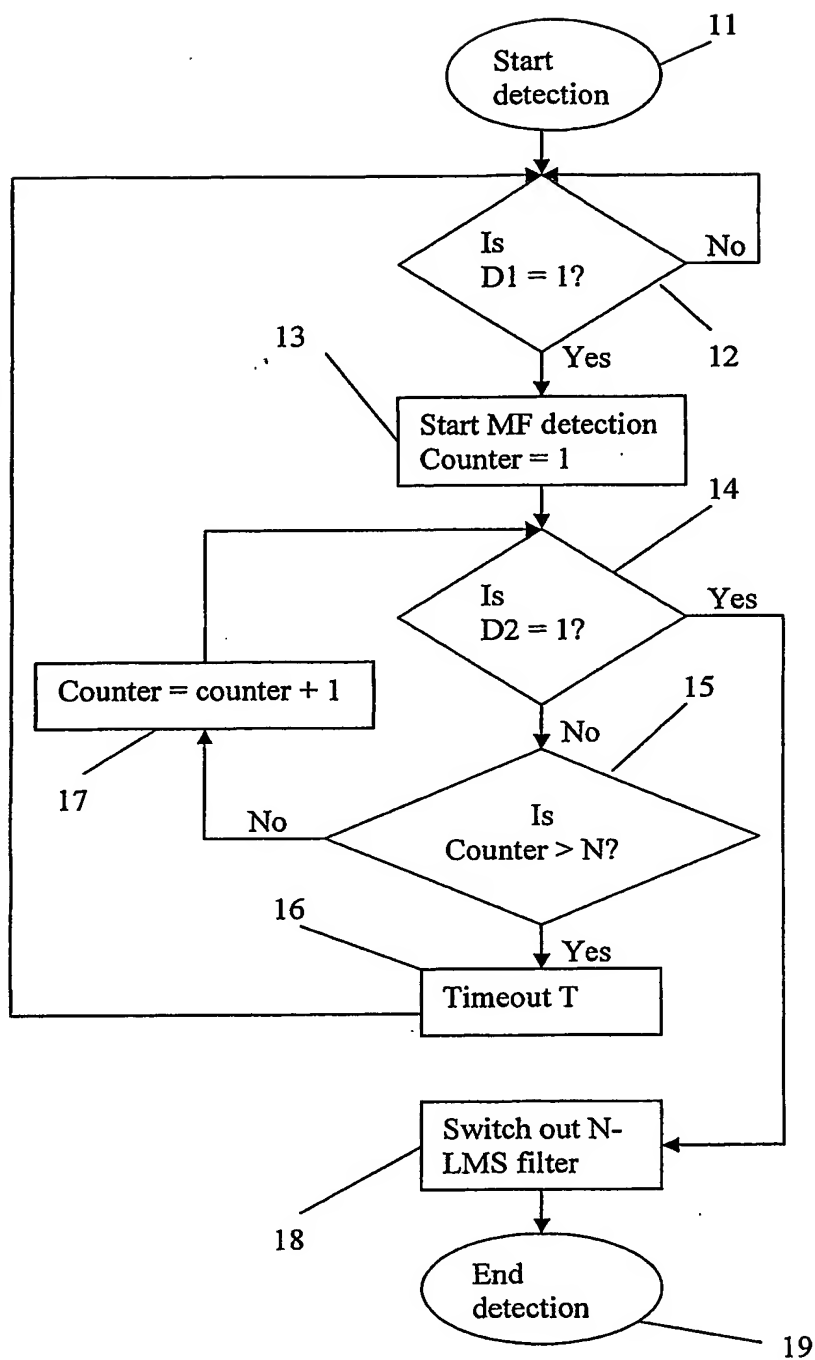


Figure 10B